Atomistic-scale investigations of hyperthermal oxygen-graphene interactions via ReaxFF molecular dynamics simulation: the gas effects

Zhiliang Cui (崔智亮) [1], *Guice Yao* (姚贵策) [1*], *Jin Zhao* (赵瑾) [2,3,1*], *Jun Zhang* (张俊) [1], *Dongsheng Wen* (文东升)[2,1,3,4]

[1]*School of Aeronautic Science and Engineering, Beihang University, Beijing, 100191, China*

[2]*School of General Engineering / International Research Institute for Multidisciplinary Science, Beihang University, Beijing, 100191, China*

[3] *Ningbo Institute of Technology, Beihang University, Ningbo, Zhejiang, 315100, China*

[4]*School of Chemical and Process Engineering, University of Leeds, Leeds, LS2 9JT*

Corresponding authors.

Email addresses:

yaoguice@buaa.edu.cn (Guice Yao), jin.zhao@buaa.edu.cn (Jin Zhao)

Abstract

Hyperthermal atomic oxygen (AO) bombardment to thermal protection system (TPS) surface has been identified to impact the aerodynamic heating significantly, due to complex chemical reactions at the gas-solid interface, e.g. surface catalysis recombination, oxidation and ablation. Previous investigations have focused on surface

temperature effects on the AO collision process, while the influence of impacting gas characteristics still remains unclear under various non-equilibrium aerodynamic conditions. This work conducts a Reactive Molecular Dynamics (RMD) study of AO collisions over graphene surface at the atomistic scale, by considering the incoming gas at different translational energy ($0.1 \leqslant E_k \leqslant 10$ eV), incident angle ($\theta = 15°, 30°, 45°, 60°, 75°, 90°$) and   O/$O_2$ ratio ($\chi_{O_2}=0.00 , 0.25, 0.50, 0.75, 1.00$). The RMD results indicate that for AO normal incidence, the predominant reactive products of O_2, CO and CO_2 molecules are produced due to the synergistic catalytic recombination and surface ablation reaction effects. A maximum recombination performance is identified around 5-eV AO incidence. For off-normal AO incidence, the recombination coefficient increases with the increase of incidence angle from 15° to 60° due to the larger perpendicular components of translational energy, and then decreases smoothly. With the increase of mole fraction of O_2, the surface reflection probabilities increases, which results in the decrease of both catalytic recombination and ablation activities . Via revealing the atomistic-scale mechanism of gas effects on the surface under hypersonic non-equilibrium conditions, . this work sheds light for the future design and optimisation of thermal protection materials.

Key Words

Catalytic recombination, surface ablation, hypersonic , reactive molecular dynamics (RMD), hyper-enthalpy collisions, graphene

1. Introduction

In low Earth orbit, the high speed compresses the air near the vehicle surface and can raise the temperature to several thousands of Kelvin through aerothermal action [1-3]. Among many gaseous species like O, N_2, O_2, Ar, He, and H, atomic oxygen (AO),

1   which is generated by UV or high temperature, is regarded as the most hazardous to the

2   flight vehicle [4-7]. Hypervelocity AOs collide to vehicles and interact both chemically

3   and mechanically with surface. Predicting these interactions with the surface is

4   important when designing the thermal protection system (TPS) to protect vehicles from

5   severe aerodynamic heating [8-11]. Therefore, gas-surface collision dynamics under

6   severe conditions have been investigated for a variety of surfaces both theoretically and

7   experimentally [12-17]. Molecular beam experiments were performed where certain

8   gas was induced and collided with various neat metallics, nonmetallic, polymers and

9   composites under different experimental conditions [18-20]. However considering the

10   multiple influential factors, a clear understanding of the AO impact effects leading to

11   the disintegration is still experimentally challenging [21-23]. To this end, molecular

12   dynamics (MD) simulations can be used as an alternative to investigate AO degradation

13   mechanisms on solid surfaces [24-27].

14   Especially ReaxFF reactive force field, which was developed by van Duin et al.

15   [28-34], can be used to simulate the formation and breaking of chemical bonds when

16   undergoes chemical and mechanical erosion, known as reactive molecular dynamics

17   (RMD). RMD investigations on hypersonic gas collisions have been further validated

18   and developed recently [35-39]. For example, Ashraf et. al. [40] used ReaxFF to

19   evaluate the disintegration of several thermosetting epoxy polymers upon hypervelocity

20   AO impact. The simulation results indicated that epoxy with aromatic curative

21   displayed higher resistance to AO impact due to its stable benzene functionality. Park

22   et. al. [41, 42] performed RMD simulation of AO collision simulations on 3C-SiC

23   structures with various surface orientations. It was successfully observed the sensitivity

24   difference according to the direction and the oxidation mechanism depending on the

25   surface temperature. Cui et. al. [43] demonstrated the atomistic oxygen colliding with

a graphite surface with an initial translational energy of 5 eV using reactive MD simulations with ReaxFF$_{C/H/O}$ force field. The simulation was validated successfully by some experimental data??, and showed that the established gas-solid interface (GSI) can be reliably used in assessing interfacial hyper-enthalpy flow reactions Majumder et. al. [44] studied the energy transfer by RMD for O_2 impingement onto a graphite surface with a fixed incident angle of 45°. The results showed that the average energy retained in the O_2 translation were linearly related to the initial translation energy. Li et. al. [45] simulated the conversion of amorphous carbon on the nickel (Ni) surface to graphene during rapid heat treatment and found that the diffusion behavior of carbon atoms was affected in the Ni layer due to the low diffusion activation energy of carbon atoms. The scattering process of N_2 impinging on graphite was also simulated to investigate the effects of angular distribution of N_2, the average translational/rotational energy and the number of rebounds [46, 47].

Previous experimental and simulation results indicate that the hyper-enthalpy collision response is not only correlated with the morphology and other properties of solid surface, e.g. temperature, but also closely dependent on the gas properties / characteristics, e.g. the collision energies, incident angle and mixing components. These gas effect, however, still remain unclear. By considering above three impacts of gas translational energy, initial incident angle and binary O/O_2 gas mixing components, the gas characteristic impacts on collisions over a graphene surface will be focused in the presented work using RMD simulation method. This simulation extends and follows a recent study of the dynamics of AO collisions with graphite surface [41].

2. Molecular Dynamics Simulation Details

The MD simulations are conducted by using LAMMPS package [48] with ReaxFF force field [28] to describe the multifield coupled interactions between the

oxygens and graphene surface. The detailed parameters of ReaxFF potentials applied

in this work can be found in the original publications [29], which has been identified to

study the oxidation phenomenon of carbon-based materials properly [30-34].

Aiming to investigate the graphene film exposed to the hyperthermal AOs, a

gas-solid heterogeneous reaction model is constructed as shown in **Figure 1**. The model

is composed of both incoming AO flux as the gas phase and a graphene plane as the

solid phase. The single-layer graphene film contains 864 carbon atoms in total with a

size of 51.16 Å × 44.30 Å, where a single oxygen atom is generated every 1.0 ps at a

random horizontal position with 5 Å above from the graphene surface. To study the

various gas effects on the hyperthermal collisions, the impinging AO flux with different

kinetic energy, incident angle and mixing compositions (binary O/O_2 mixture) are

considered in this work with graphene film at the fixed temperature at xxx Kelvin.

Moreover, to ensure the centroid position of the single-layer graphene is relatively

stable during the continuous incidence of AOs, the position constraints are added by

fixing the carbon atoms at the four corners of the graphene.
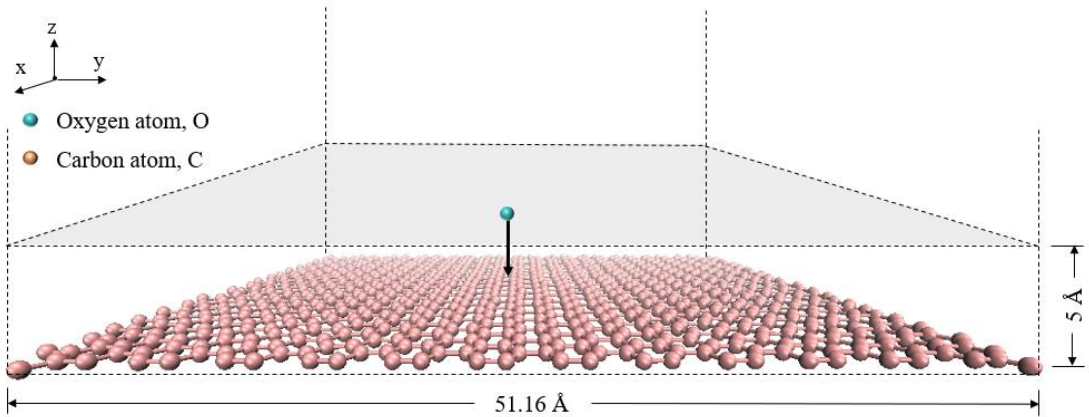
Figure 1 The initial schematic configuration of hyper-enthalpy AOs colliding with graphene film

The whole system energy is firstly minimized to the equilibrium state. After

energy minimization, the Berendsen method was used as the thermostat to control the

graphene film temperature under the NVT ensemble. Periodic boundary conditions are

applied for both *x*- and *y*- directions parallel to the graphene, and reflective boundary

conditions were used in the *z* direction. All the simulations are carried out with a period

of 500 ps with a timestep of 0.10 fs. The trajectories of each atom in the model are

collected every 1000 steps during the AO incidence process for post processing and

analysis.

3 Results and Discussion

3.1 The effects of the AO impinging translational energy

Aiming to investigate the effect of kinetic energy for AOs colliding on the

graphene surface, eight models were constructed with oxygens impinging normal to the

graphene surface associating with their translation energy of 0.1, 1.0, 2.0, 4.0, 5.0, 6.0,

8.0, 10.0 eV, respectively.

The surface morphology of the graphene film is monitored by tracing the

oxygen trajectories firstly, as shown in **Figure 2**. It can be observed that the atomic

oxygens are adsorbed on the active sites during the continuous impingement for all the

models, saturating the graphene surface gradually. The final saturation number of the

adsorbed oxygens is almost monotonously increasing with the increase of oxygen

impinging translational energy. Associating with the visualization of the final

configuration snapshots as illustrated in **Figure 2(b)**, various small molecules are

generated and gasified during the collisions, e.g. O_2, CO, CO_2, etc. Obvious

fragmentations can be observed for the cases with larger translational energy of
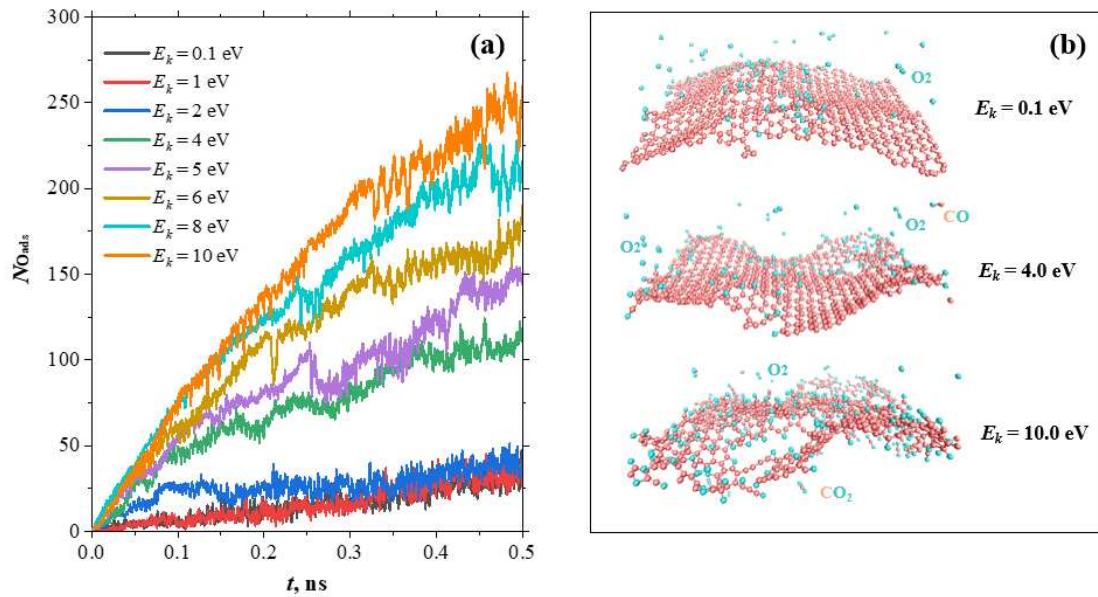
incoming AO flux.

6   To identify the detailed hyperthermal collision process, the statistic analysis of

7 various gasified components and the configuration evolutions are illustrated in **Figure**

8 **3** for the case with impingement translational energy of 10.0 eV: three kinds of

9 components are released from the surface, where the oxygen molecules (O_2) are

10 generated as the majority in this case due to the recombination from two incoming

11 atomic oxygens with graphene acting as the catalyzing surface. The carbon atoms are

12 lost from the original graphene film structure caused by the impact of high enthalpy

13 oxygen atoms, forming the oxidized products of carbon dioxide and carbon monoxide

14 molecules, leaving multiple voids on the graphene surface as shown in **Figure 3(b)**.

15
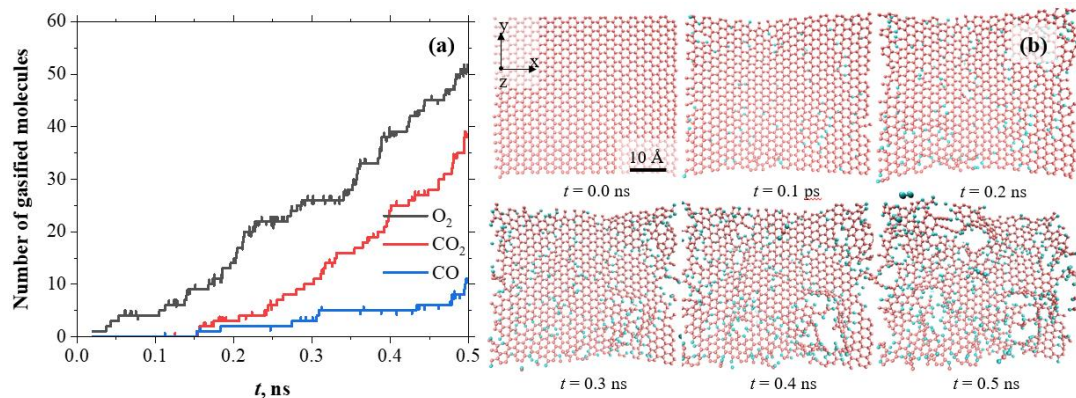
Figure 3 The collision process of impinging oxygens with translational energy of 10.0 eV on the graphene surface. (a) The statistical number of each gasified composition with the evolution of time; (b) The configuration snapshots of graphene film with the evolution of time

The surface catalytic characteristics of graphene surfaces under various impinging translational kinetic energy of oxygen atoms are analyzed in **Figure 4**. The surface catalytic recombination coefficient γ of molecular oxygen species as monitored in **Figure 4(b)** is derived from as the ratio of the number flux of reacting particles to the number flux of impinging particles [49]. Under the incidence of various AO kinetic energy, the catalytic recombination coefficient γ increases gradually with time and reaching equilibrium with minor oscillations after about 300 ps. The averaged catalytic recombination coefficient γ_{ave} is determined through averaging the instantaneous values in the last 50.0 ps, as presented in **Figure 4(c)**. A peak value of the averaged catalytic recombination coefficient γ_{ave} is surprisingly found for the model with incoming oxygen translational energy of 5.0 eV, with its maximum γ_{ave} value around 0.23. This is almost 4 times greater than the minimum catalytic recombination coefficient of 0.06 for the incoming oxygen translational energy of 0.1 eV. This is due to the factowhen the AO kinetic energy is greater than 5.0 eV, the oxygen tends to break more epoxy bonds on the graphene surface, combining with carbon atoms to form CO_2 or CO molecules, as presented in **Figure 5**. Therefore, the number of recombined oxygen molecules decreases, leading to the decrease of the catalytic recombination coefficient. The similar

1 result can be found from the conclusions by Vinogradov and Singh et al. [50, 51].

2
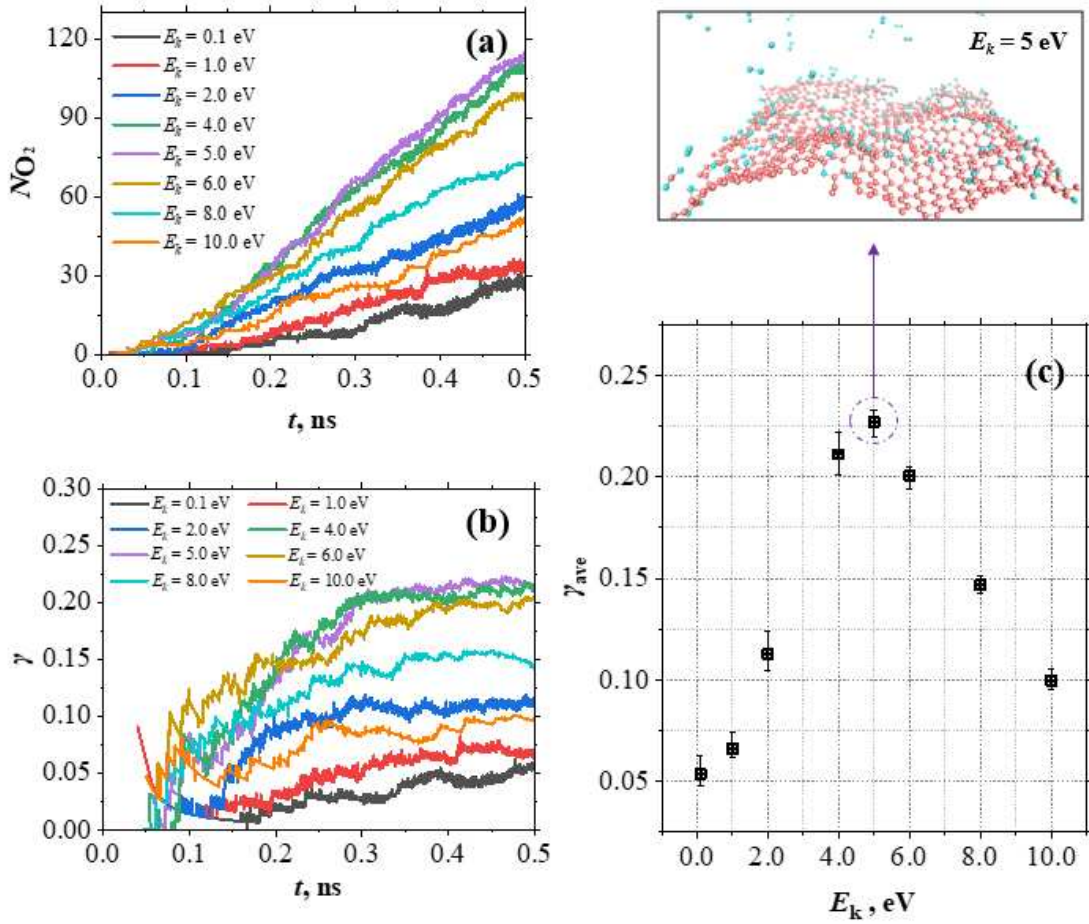
3
4 **Figure 4** The surface catalytic characteristics of graphene surfaces under various impinging
5 translational kinetic energy of oxygen atoms. (a) The number of recombined oxygen molecules
6 with the evolution of time; (b) The instantaneous statistics of the surface catalytic
7 recombination coefficient; (c) The averaged surface catalytic recombination coefficient for the
8 models with different oxygen impinging translational energy.
9
10
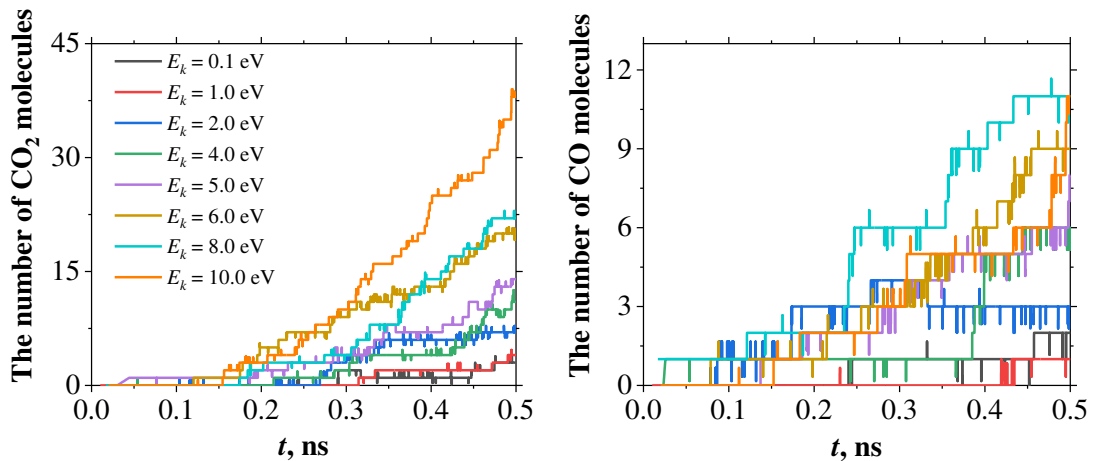
11
12   (a) The number of gasified CO_2 molecules   (b) The number of gasified CO molecules
13 **Figure 5** The formation process of both carbon dioxide and carbon monoxide molecules as a

function of time with various impinging translational energy. (a) The number of gasified CO_2 molecules (b) The number of gasified CO molecules

The production process of both carbon dioxide and carbon monoxide molecules for all the eight models can be found in **Figure 5**. The ratio of the lost carbon atoms and the average ablation rate k can be consequently derived as shown in **Figure 6**. Differing from the non-linear relations between the catalytic recombination coefficients and incoming translational energy, there is a significantly positive linear correlation between the translational energy and erosion rate k.

(a) (b)
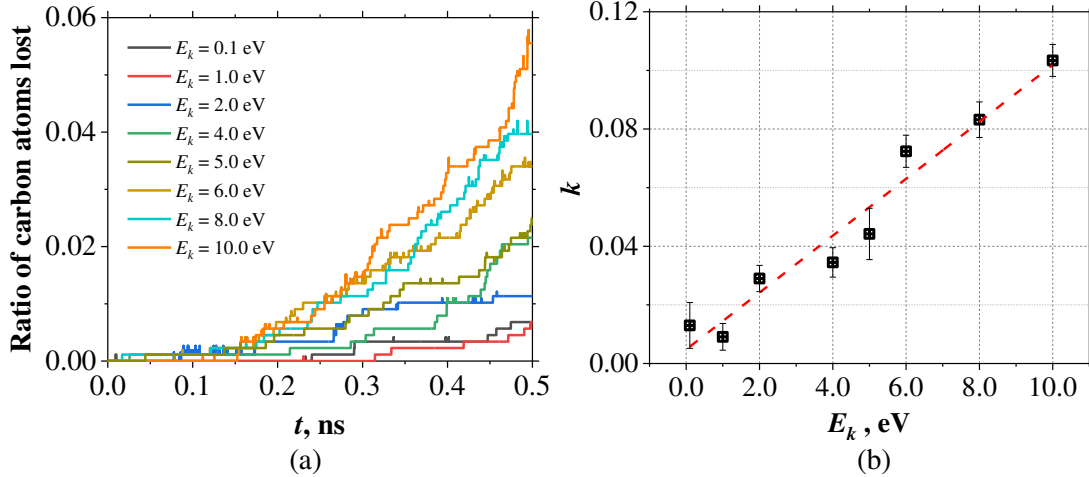
Figure 6. The effect of incoming kinetic energy on the erosion characteristics of graphene. (a) The ratio of carbon atoms lost from graphene surface as a function of time; (b) The variations of erosion rate as a function of impinging translational energy.

3.2 The effect of AO incident angle on graphene erosion

The impact of AO incident angle on the erosion process of graphene is investigated through keeping the incoming translational energy of 5.0 eV as a constant value in this section. In comparison with the normal incidence model ($\theta = 90°$), another five models are established with fixed initial incident angles θ of 15°, 30°, 45°, 60° and 75°, respectively. After a period of 500 ps RMD simulation, the surface catalysis and erosion characteristics are further analyzed.

equilibrium $t = 100$ ps $t = 200$ ps   equilibrium $t = 100$ ps $t = 200$ ps

$t = 300$ ps $t = 400$ ps $t = 500$ ps $t = 300$ ps $t = 400$ ps $t = 500$ ps

(a) $\theta = 15°$ (b) $\theta = 90°$

Figure 7 The configuration evolution of graphene as a function of time, with oxygen incident angle of (a) $\theta = 15°$ and (b) $\theta = 90°$

Taking the AO incident angles θ of 15° and 90° as examples, the configuration evolutions of graphene as a function of time are illustrated in **Figure 7**. It can be visualized that there is a notable difference for the final morphology at 500 ps between these two models: more voids due to the hyper-enthalpy collisions are observed when AOs are incoming normal to the surface, compared with the oblique incidence condition. To quantitatively denote the ablation magnitude, the effect of AO incident angle on the erosion process is identified as shown in **Figure 8**. With the increase of the incident angles of oxygen atoms, the ablation rates of graphene surface are accelerated. The number of broken carbon-carbon bonds increases with the incident angles of AO flux, due to the fact that energy component of the oxygen atoms in the direction perpendicular to the graphene plane increases.

Figure 8 The effect of atomic-oxygen incident angle on the graphene erosion process. (a) Number of C-C bond broken with the evolution of time and (b) total number of C-C bond broken for various incident angle θ situations

Though a monotonous incline erosion rate with the increase of AO incident angle, different trend is emerged for the variations of graphene surface catalytic characteristics, as shown in **Figure 9**. With various AO incident angles, the catalytic recombination coefficient γ increases with time, and is in oscillating equilibrium after about 400 ps from **Figure 9(a)**. The averaged recombination coefficient after equilibrium γ_{ave} is calculated as indicated in **Figure 9(b)**: A peak value of γ_{ave} in relation to the various incidence angle θ of AOs is emerged at around 60° as seen in **Figure 9(b)**. Possible reason can be emphasized through visualizing the oxygen trajectory: with the increase of incident angle θ from 0° to 60°, the probability for impinging oxygen atoms to hit the preadsorbed oxygen atoms at the active sites of graphene surface is enhanced, recombining into oxygen molecules and releasing out; as the incident angle θ continuously increasing greater than 60°, the incoming AO flux tends to change their behaviors from the recombination activities into the situations of elastic collisions and reflections, due to larger perpendicular component of kinetic energy normal to the graphene surface. Instead of recombing into new molecular oxygens, they scatter away by the surface as a reflector. Similar conclusion of this non-linear relation has also been

1 drawn by Norman et al. [52] aiming at the impact of oxygen atoms on the silica surface

2 with various incident angles.

(a)   (b)
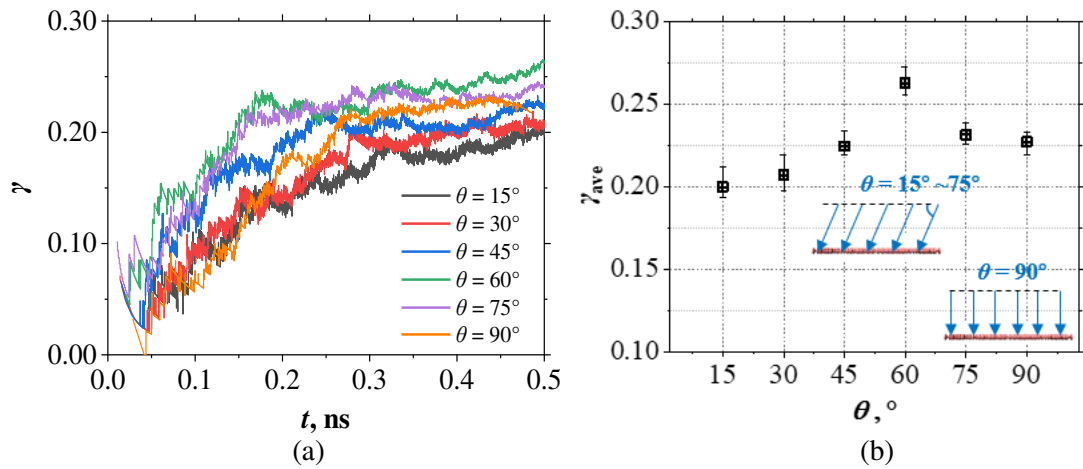
Figure 9 The effect of atomic-oxygen incident angle on the graphene surface catalysis. (a) Instant recombination coefficient γ with the evolution of time and (b) the averaged recombination coefficient γ_{ave} with various incident angle θ situations

3.3 The effects of binary O/O₂ gas mixture on the graphene erosion process

10   The effects of binary O/O_2 gas mixture on the graphene erosion process is

11 focused on with various mole fraction ratio of oxygen molecules χ_{O_2} from 0.00 (pure

12 AO flux as incoming flow) to 1.00 in this session. Same kinetic energy of impinging

13 collisions with 5.0 eV are employed for comparisons.
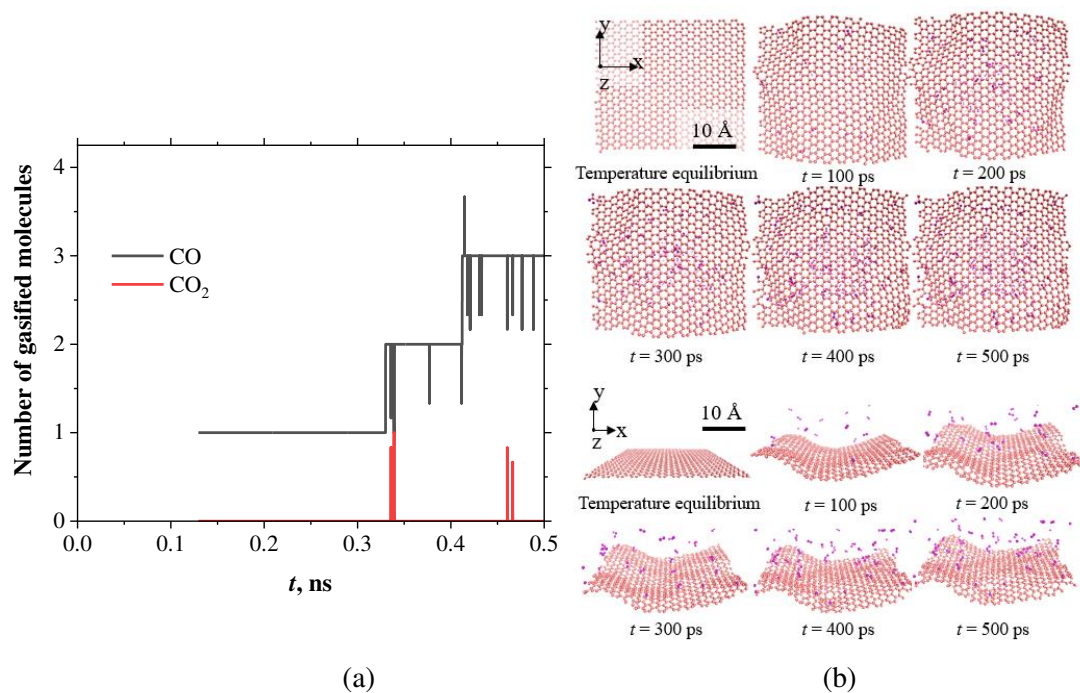
(a)   (b)

1 **Figure 10** The interactions of oxygen molecules impinging to the graphene surface (a) The
2 number of various gasified molecules as a function of time for the pure molecular oxygen flow
3 impingements, χ_{O_2} = 1.00 and (b) the final morphology of graphene after the 500-ps collisions
4

5 Taking the mole fraction χ_{O_2} = 1.00 of the pure molecular oxygen flow

6 impingements as an example, a distinct difference can be noticed that only a tiny

7 amount of CO and CO_2 molecules are gasified as shown in **Figure 10** after continuous

8 collisions for 500 ps, compared with pure AO impingement (χ_{O_2} = 0.00) as shown in

9 **Figure 5(a, b)** when same E_k is applied. Hence, the erosion performance of graphene

10 surface is found to be weaker in this case. To justify this comparison, various mole

11 fractions of binary O/O_2 gas mixture flow stream collisions on the graphene surface is

12 presented in **Figure 11**. The production process of CO and CO_2 gasified molecules with

13 various χ_{O_2} inlet boundary can be counted quantitively as a function of time.
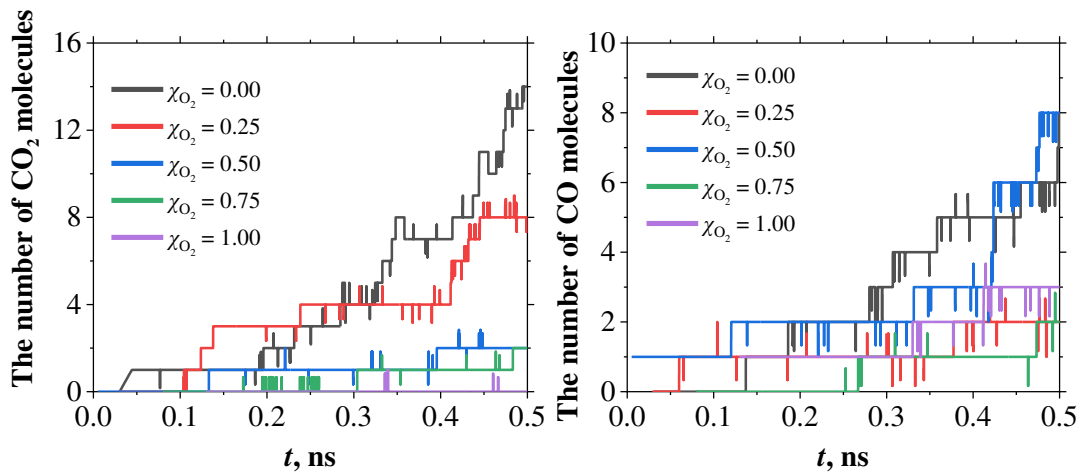
14
15
16   (a) The number of gasified CO_2 molecules   (b) The number of gasified CO molecules
17 **Figure 11** The formation process of both carbon dioxide and carbon monoxide molecules as a
18 function of time with various mole fraction ratio of binary O/O_2 gas mixture. (a) The number
19 of gasified CO_2 molecules (b) The number of gasified CO molecules
20

21 The ablation rates of graphene surface are consequently calculated as shown in

22 **Figure 12**. With the increase of molecular oxygen mole fraction χ_{O_2} in the binary

23 species mixture, the ablation process is decelerated due to less carbon lost rate from the

24 graphene surface. It is indicated that the double bonds in oxygen molecules are more

1 stable and stronger than the C-O and C-C single bonds under various reaction

2 conditions during the collisions. The morphology evolutions at the gas/solid interface

3 as a function of time are illustrated for the inlet conditions χ_{O_2} of 0.25 and 0.75,

4 respectively, in **Figure 13**.

(a)   (b)
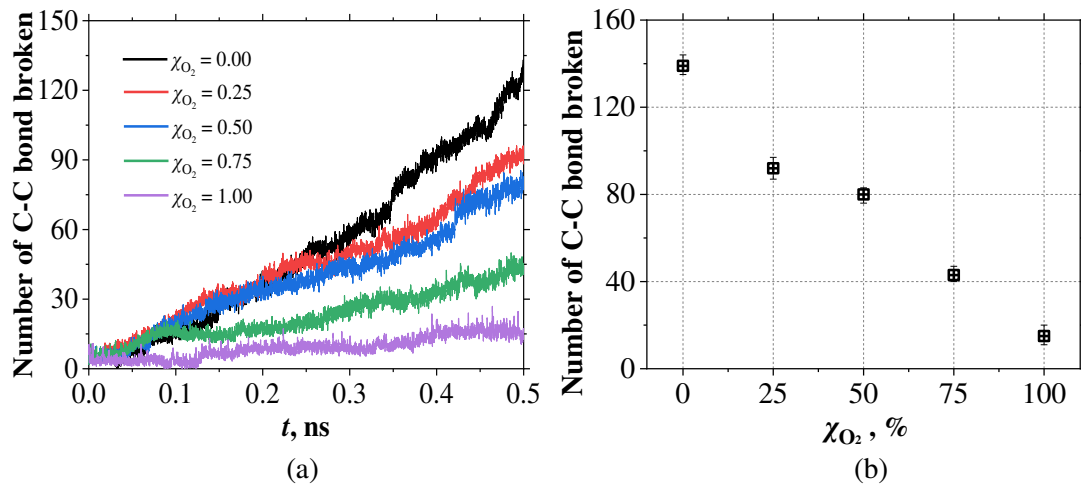
7 **Figure 12** The effect of mole fraction ratio of binary O/O_2 gas mixture on the graphene erosion
8 process. (a) Number of C-C bond broken with the evolution of time and (b) total number of C-
9 C bond broken for various molecular oxygen mole fraction χ_{O_2} situations
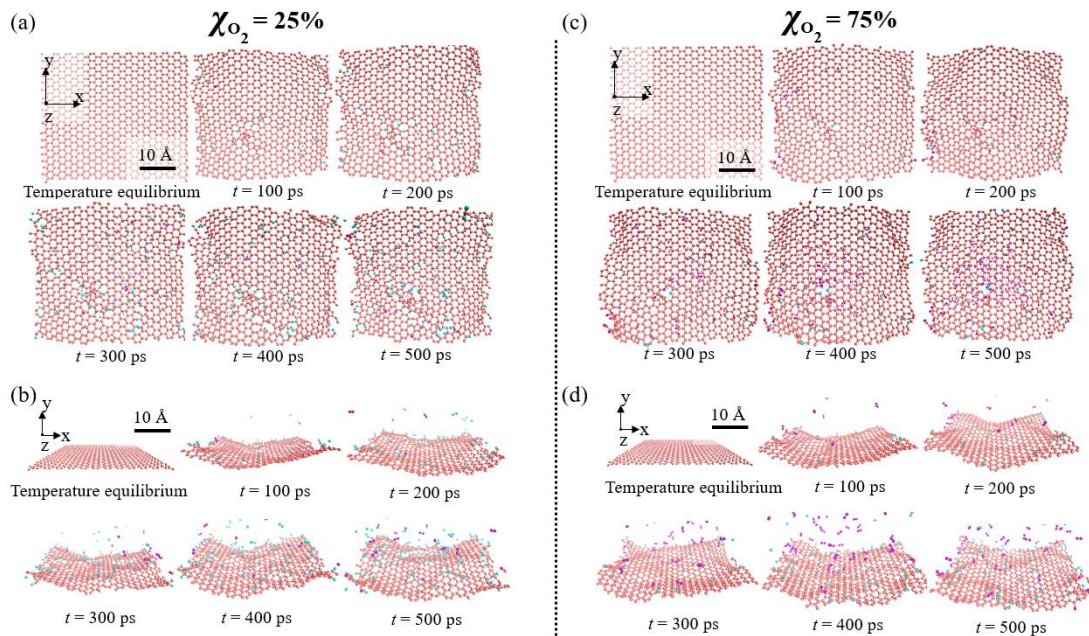
12 **Figure 13** The morphology evolutions at the gas/solid interface as a function of time with the
13 inlet χ_{O_2} conditions of (a, b) 0.25 and (c, d) 0.75.

15   The last but not the least, the surface catalysis characteristics of graphene under

16 various binary O/O_2 gas mixture ratio are analyzed as shown in **Figure 14**. It is

1   indicated that the recombination possibility is declined nonlinearly with the increasing

2   amount of O_2 components in the binary mixture impingement flow. As a result, the

3   average recombination coefficient for the inlet condition χ_{O_2} of 0.00 is enumerated as a

4   value of 0.23, while for χ_{O_2} varying from 0.25 to 1.00, the γ_{ave} can be obtained through

5   our RMD calculations with a value of 0.21, 0.18, 0.11 and 0.00, respectively.

6
7   (a)   (b)
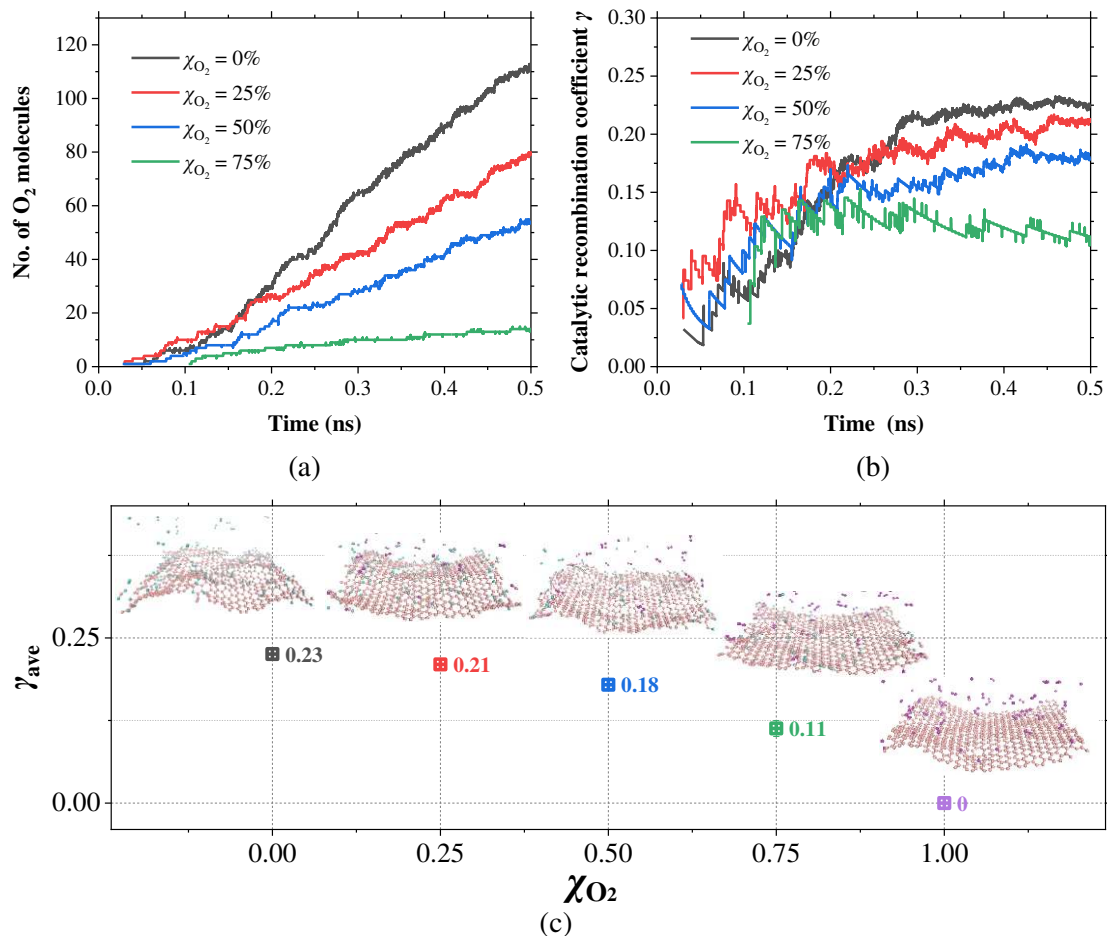
8
9   (c)
10   **Figure 14** The effect of mole fraction ratio of binary O/O_2 gas mixture on the graphene surface
11   catalysis. (a) The production process of recombined oxygen molecules with the evolution of
12   time; (b) Instantaneous recombination coefficient γ with the evolution of time and (c) the
13   averaged recombination coefficient γ_{ave} with various inlet χ_{O_2} conditions
14
15
16   **4. Conclusions**

17   The gas effect on the hyper-enthalpy impingement on the graphene surface are

18   investigated using RMD simulation method with ReaxFF reactive force field. The

19   surface catalysis and erosion processes are analysed by considering the gas effect with

various incoming translational energy, incident angle and binary mixture component ratio, respectively. The results indicate that For AO normal incidence, the predominant reactive products of O_2, CO and CO_2 molecules are detected due to the catalytic recombination and surface ablation reaction pathways, respectively. A maximum recombination performance is identified around 5-eV AO incidence with within the large investigated range of 0.1 and 10 eV. Both AO adsorption and reflection processes are recognized during the incidence process, and the adsorption probabilities increase monotonously with an incline of translational energy. O colliding onto a denser O-preadsorbed surface, produces more O_2 molecules. However, with AO translational energy greater than 5 eV, the stronger atom–surface collisions result in more intense reflection and erosion phenomenon with carbon atom lost from graphene, which diminishes further recombination rate increment.

Analogous to the above mechanism, for off-normal AO incidence, the recombination coefficient grows with an increase of incidence angle from 15° to 60° due to the larger perpendicular components of translational energy, and then decreases smoothly. For incoming binary gas mixture containing O and O_2, the greater mole fraction of O_2 would enhance reflection probabilities, while both catalytic recombination and ablation characteristics are found to be restrained. This work can provide an atomistic-scale mechanism origin insight on the hypersonic non-equilibrium effects on the thermal boundary layer response due to the gas characterization impacts.

Data Availability

The data that support the findings of this study are available from the corresponding author upon reasonable request.

References

[1] Z. Hu, S. Meng, F. Yi, J. Li, and C. Xu, "Oxyacetylene ablation resistance of continuous gradient ceramic–polymer composite," Corrosion Sci. 179: 109050 (2021).

[2] R. Ding, J. Wang, F. He, M. Wang, Y. Luan, G. Dong, and L. Tang, "Numerical investigation on a double layer combined cooling structure for aerodynamic heat control of hypersonic vehicle leading edge," Appl. Therm. Eng. **169**: 114949 (2020).

[3] W. Li, G. Fang, W. Li, J. Liang, and S. Meng, "Numerical investigation of mesoscopic volumetric ablation of 3D braided charring composites," Appl. Therm. Eng. **181**: 116016 (2020).

[4] Z. Yuan, S. Huang, X. Gao, and J. Liu, "Effects of surface-catalysis efficiency on aeroheating characteristics in hypersonic flow," J. Aerosp. Eng. **30**(3): 04016086 (2017).

[5] I. Kim, Y. Yang, and G. Park. "Effect of titanium surface roughness on oxygen catalytic recombination in a shock tube," Acta Astronaut. **166**: 260 (2020).

[6] G. Colonna, F. Bonelli, and G. Pascazio, "Impact of fundamental molecular kinetics on macroscopic properties of high-enthalpy flows: The case of hypersonic atmospheric entry," Phys. Rev. Fluids **4**(3): 033404 (2019).

[7] G.V. Candler, "Rate effects in hypersonic flows," Annu. Rev. Fluid Mech. **51**: 379 (2019).

[8] K. Swaminathan-Gopalan, A. Borner, V.J. Murray, S. Poovathingal, T.K. Minton, N.N. Mansour, and K.A. Stephani, "Development and validation of a finite-rate model for carbon oxidation by atomic oxygen," Carbon, **137**: 313 (2018).

[9] G. Ceglia, A. Del Vecchio, U. Koch, B. Esser, and A. Gülhan, "Two-Photon Laser-Induced Fluorescence Measurements of Atomic Oxygen Density in Hypersonic Plasma Flow," J. Thermophys. Heat Transf. **33**(2): 292 (2019).

[10] N.K. Gopinath, G. Jagadeesh, and B. Basu, "Shock wave-material interaction in ZrB2–SiC based ultra-high temperature ceramics for hypersonic applications," J. Am. Ceram. Soc. **102**(11): 6925 (2019).

[11] J.H. Chae, T.K. Mankodi, S.M. Choi, R.S. Myong, "Combined effects of thermal non-equilibrium and chemical reactions on hypersonic air flows around an orbital reentry vehicle," Int. J. Aeronaut. Space Sci. 1-15 (2019).

[12] G.J. Kroes, M. Pavanello, M. Blanco-Rey, M. Alducin, and D.J. Auerbach, "Ab initio molecular dynamics calculations on scattering of hyperthermal H atoms from Cu (111) and Au (111)," J. Chem. Phys. **141**(5): 054705 (2014).

[13] I. Kim, and G. Park, "Experimental study of oxygen catalytic recombination on a smooth surface in a shock tube," Appl. Therm. Eng. **156**: 678 (2019).

[14] W. Zhu, H. Gong, Y. Han, M. Zhang, and A.C.T. van Duin, "Development of a Reactive Force Field for Simulations on the Catalytic Conversion of C/H/O Molecules on Cu-Metal and Cu-Oxide Surfaces and Application to Cu/CuO-Based Chemical Looping," J. Phys. Chem. C **124**(23): 12512 (2020).

[15] L. Krumbein, K. Anggara, M. Stella, T. Michnowicz, H. Ochner, S. Abb, and S. Rauschenbach, "Fast molecular compression by a hyperthermal collision gives bond-selective mechanochemistry," Phys. Rev. Let. **126**(5): 056001 (2021).

[16] J.W. Streicher, A. Krish, R.K. Hanson. "Vibrational relaxation time measurements in shock-heated oxygen and air from 2000 K to 9000 K using ultraviolet laser absorption," Phys. Fluids **32**(8): 086101 (2020).

[17] I.C. Gerber, and P. Serp, "A theory/experience description of support effects in carbon-supported catalysts," Chem. Rev. **120**(2): 1250 (2019).

[18] K.D. Gibson, S. J. Sibener, H. P. Upadhaya, A. L. Brunsvold, J. Zhang, T. K. Minton, and D. Troya, "Hyperthermal Ar Atom Scattering from C(0001) Surface," J. Chem. Phys. **128**,

224708 (2008).

[19] K.S. Prata, T.K. Minton, and T.E. Schwartzentruber. "Air-Carbon Ablation Model for Hypersonic Flight from Molecular Beam Data," AIAA Scitech Forum. **2021**: 0925 (2021).

[20] X. Zhou, Y. Zhang, H. Guo, and B. Jiang, "Towards bridging the structure gap in heterogeneous catalysis: the impact of defects in dissociative chemisorption of methane on Ir surfaces," Phys. Chem. Chem. Phys. **23**(7): 4376 (2021).

[21] V.J. Murray, and T.K. Minton, "Gas-surface interactions of atomic nitrogen with vitreous carbon," Carbon, **150**: 85 (2019).

[22] V.J. Murray, P. Recio, A. Caracciolo, C. Miossec, N. Balucani, P. Casavecchia, and T.K. Minton, "Oxidation and nitridation of vitreous carbon at high temperatures," Carbon, **167**: 388 (2020).

[23] O. Galparsoro, H.F. Busnengo, A.E. Martinez, J.I. Juaristi, M. Alducin, and P. Larregaray, "Energy dissipation to tungsten surfaces upon hot-atom and Eley–Rideal recombination of H_2," Phys. Chem. Chem. Phys. **20**(33): 21334 (2018).

[24] N. Andric, and P. Jenny, "Molecular dynamics investigation of energy transfer during gas-surface collisions," Phys. Fluids **30**(7): 077104 (2018).

[25] S. Yuan, H. Zhang, and S. Yuan, "Atomistic insights into resistance to oxidation of Si (111) grafted different organic chains," Comput. Mater. Sci. **191**: 110336 (2021).

[26] J. Zhao, G. Yao, and D. Wen, "Salinity-dependent alterations of static and dynamic contact angles in oil/brine/calcite systems: a molecular dynamics simulation study," Fuel, **272**: 117615 (2020).

[27] J. Zhao, G. Yao, S.B. Ramisetti, R.B. Hammond, and D. Wen, "Molecular dynamics investigation of substrate wettability alteration and oil transport in a calcite nanopore," Fuel, **239**: 1149 (2019).

[28] A.C.T. van Duin, S. Dasgupta, F. Lorant, and W. A. Goddard, "ReaxFF: A reactive force field for hydrocarbons," J. Phys. Chem. A **105**, 9396 (2001).

[29] K. Chenoweth, A.C.T. van Duin, and W. A. Goddard, "ReaxFF reactive force field for molecular dynamics simulations of hydrocarbon oxidation," J. Phys. Chem. A **112**, 1040

(2008).

[30] S.G. Srinivasan, and A.C.T. van Duin. "Molecular-dynamics-based study of the collisions of hyperthermal atomic oxygen with graphene using the ReaxFF reactive force field," J. Phys. Chem. A **115**.46: 13269 (2011).

[31] S. Poovathingal, T.E. Schwartzentruber, S.G. Srinivasan, and A.C.T. van Duin, "Large scale computational chemistry modeling of the oxidation of highly oriented pyrolytic graphite," J Phys Chem A **117**(13): 2692 (2013).

[32] A. Rahnamoun, and A.C.T. van Duin. "Reactive molecular dynamics simulation on the disintegration of Kapton, POSS polyimide, amorphous silica, and teflon during atomic oxygen impact using the reaxff reactive force-field method," J. Phys. Chem. A **118**(15): 2780 (2014).

[33] S.G. Srinivasan, A.C.T. van Duin, and P. Ganesh, "Development of a ReaxFF potential for carbon condensed phases and its application to the thermal fragmentation of a large fullerene," J. Phys. Chem. A **119**(4): 571 (2015).

[34] S.G. Srinivasan, and A.C.T van Duin, "Direction dependent etching of diamond surfaces by hyperthermal atomic oxygen: A ReaxFF based molecular dynamics study," Carbon, **82**: 314 (2015).

[35] D. Hou, Z. Lu, X. Li, H. Ma and Z. Li. "Reactive molecular dynamics and experimental study of graphene-cement composites: Structure, dynamics and reinforcement mechanisms," Carbon; **155**: 188 (2017).

[36] G. Füchsel, X. Zhou, B. Jiang, J. I. Juaristi, M. Alducin, H. Guo, and G.J. Kroes, "Reactive and nonreactive scattering of HCl from Au (111): An ab initio molecular dynamics study," J. Phys. Chem. C **123**(4): 2287 (2019).

[37] X. Zhou, L. Zhang and B. Jiang. "Hot-atom-mediated dynamical displacement of CO adsorbed on Cu (111) by incident H atoms: An ab initio molecular dynamics study," J. Phys. Chem. C **122**(27): 15485 (2018).

[38] X.Z. Jiang, M. Feng, W. Zeng, K.H. Luo, "Study of mechanisms for electric field effects on ethanol oxidation via reactive force field molecular dynamics," Proc. Combust. Inst.

37(4): 5525 (2019).

[39] C. Jian, J.J. Adams, J.C. Grossman, and N.Ferralis, "Carbon fiber synthesis from pitch: Insights from ReaxFF based molecular dynamics simulations," Carbon, **176**: 569 (2021).

[40] C. Ashraf, A. Vashisth, C.E. Bakis and A.C.T. van Duin, "Reactive Molecular Dynamics Simulations of the Atomic Oxygen Impact on Epoxies with Different Chemistries," J. Phys. Chem. C **123**(24): 15145 (2019).

[41] T. Park, C. Park, J Jung and G.J. Yun, "Investigation of Silicon Carbide Oxidation Mechanism Using ReaxFF Molecular Dynamics Simulation," J. Spacecr. Rockets **57**(6): 1328 (2020).

[42] I. Kim, S. Lee, J.G. Kim and G. Park, "Analysis of nitrogen recombination activity on silicon dioxide with stagnation heat-transfer," Acta Astronaut. **177**: 386 (2020).

[43] Z. Cui , J. Zhao, L. He, H. Jin, J. Zhang and D. Wen, "A reactive molecular dynamics study of hyperthermal atomic oxygen erosion mechanisms for graphene sheets," Phys. Fluids **32**(11): 112110 (2020).

[44] M. Majumder, K.D. Gibson, S.J. Sibener and W.L. Hase, "Chemical Dynamics Simulations and Scattering Experiments for O_2 Collisions with Graphite," J. Phys. Chem. C **122**, 16048 (2018).

[45] X. Li, A. Wang and K.R. Lee, "Transformation of amorphous carbon to graphene on low-index Ni surfaces during rapid thermal processing: a reactive molecular dynamics study," Phys. Chem. Chem. Phys. **21**, 2271 (2019).

[46] M. Majumder, H.N. Bhandari, S. Pratihar and W.L. Hase, "Chemical dynamics simulation of low energy N2 collisions with graphite," J. Phys. Chem. C **122**, 612 (2018).

[47] N.A. Mehta, V.J. Murray, C. Xu, D.A. Levin and T.K. Minton, "Nonreactive scattering of N2 from layered graphene using molecular beam experiments and molecular dynamics," J. Phys. Chem. C **122**, 9859 (2018).

[48] S. Plimpton, P. Crozier and A. Thompson, "LAMMPS-large-scale atomic/molecular massively parallel simulator," Sandia National Laboratories, **18**: 43 (2007).

[49] R. Goulard, "On catalytic recombination rates in hypersonic stagnation heat transfer," J.

1 Jet Propul. **28**(11): 737 (1958).

2 [50] N. A. Vinogradov, K. Schulte, M. L. Ng, A. Mikkelsen, E. Lundgren, N. Martensson, and

3 A. Preobrajenski, "Impact of atomic oxygen on the structure of graphene formed on Ir

4 (111) and Pt (111)," J. Phys. Chem. C **115**, 9568 (2011).

5 [51] V. Singh, D. Joung, L. Zhai, S. Das, S. I. Khondaker, and S. Seal, "Graphene based

6 materials: past, present and future," Prog. Mater. Sci. **56**, 1178 (2011).

7 [52] P. Norman, and T. Schwartzentruber, "A finite-rate model for oxygen-silica catalysis

8 through computational chemistry simulation," American Institute of Physics, (2012).